Brillouin light scattering study of Fe/Cr/Fe (211) and (100) trilayers

M. Grimsditch, S. Kumar, and Eric E. Fullerton
Materials Science Division, Argonne National Laboratory, Argonne, Illinois 60439
(Received 15 January 1996)

The magnitude of the bilinear and biquadratic interlayer coupling strengths between Fe layers separated by Cr spacer layers is investigated by means of Brillouin light scattering, magneto-optic Kerr rotation, and magnetoresistance techniques. A data analysis scheme, which treats all three data sets on an equal footing, yields self-consistent anisotropy and interlayer coupling parameters extracted independently from the three techniques. The values of the bilinear and biquadratic coupling strengths are compared for simultaneously grown (211) and (100) Fe/Cr samples. The approach not only provides reliable values for the coupling strengths but also highlights the complementarity of these techniques in uniquely determining the magnetic parameters. [S0163-1829(96)03630-2]

I. INTRODUCTION

Many systems consisting of magnetic layers separated by nonmagnetic layers exhibit oscillatory interlayer coupling across the nonmagnetic spacer layers.[1] The coupling oscillates periodically between ferromagnetic and antiferromagnetic (AF) with increasing spacer-layer thickness in the nanometer scale region. The oscillatory nature of the coupling is explained by RKKY treatments of the spacer layer, the resulting period being inversely proportional to the length of spanning vectors which join extremal points of the Fermi surface normal to the layering direction. In most treatments of the RKKY theory, it is assumed that the coupling is Heisenberg-like of the form $-J_1\mathbf{m}_1\cdot\mathbf{m}_2$ so that only ferromagnetic or AF coupling is possible. However, it has been observed that when J_1 is small, the magnetic moments of the layers sometimes align at 90° with respect to each other [e.g., Fe/Cr(001) (Ref. 2) or Fe/Al(001) (Ref. 3)]. This type of coupling can be described by introducing a phenomenological interlayer coupling term $-J_2(\mathbf{m}_1\cdot\mathbf{m}_2)^2$, where J_2 is the biquadratic coupling constant. This type of coupling has been attributed to either intrinsic properties of the spacer layer[1,4] or to a variety of extrinsic factors, such as paramagnetic impurities within the spacer layers[4] or dipolar fields resulting from rough interfaces.[5] For Fe/Cr(100) superlattices, the presence of biquadratic coupling has been attributed to fluctuations in the Cr layer thickness which average out the short-period oscillations in Cr(100).[4]

Here we present an investigation aimed at studying the nature of the coupling in (211)-oriented Fe/Cr samples. Previous studies of Fe/Cr(211) superlattices have found that the bilinear interlayer coupling oscillates in sign with the same period (18 Å), phase, and strength as similarly prepared Fe/Cr(100) superlattices.[6] This rather isotropic behavior has been attributed to spanning vectors across a ''lens'' feature of the bulk Cr Fermi surface.[7] In the superlattice studies, the interlayer coupling strength was determined from the saturation field of the magnetic hysteresis loops, and no attempt was made to separate bilinear and biquadratic coupling contributions. Although it is straightforward to determine the period of the oscillatory coupling, a more difficult problem is obtaining reliable quantitative values of the interlayer coupling strengths. Since Fe(211) layers possess a strong in-plane uniaxial anisotropy, the presence of biquadratic coupling cannot be directly determined merely from an observed 90° alignment of adjacent layers, but, requires quantitative analysis of the magnetization and spin-wave spectra. We have combined magnetization, magnetoresistance (MR), and Brillouin light scattering (BLS) measurements to quantitatively determine both the interlayer coupling constants and the anisotropies in a manner similar to that used by Krebs *et al.*[8] for (100)-Fe/Cr/Fe trilayers. We find quantitative agreement between anisotropy and interlayer coupling constants extracted using the three techniques independently. The only other determination of biquadratic coupling in a uniaxial system we are aware of is by Elmers *et al.*,[9] who used a novel geometry to study (110)-Fe/Cr/Fe trilayers.

We focus mainly on the results and analysis of our (211)-Fe films and (211)-Fe/Cr/Fe trilayers. Results on (001) films and trilayers are presented with little emphasis on the analysis, since they follow closely the methods used for the (211) samples. Results for the two orientations are contrasted and compared with magnetization results for superlattices. In superlattices, however, there are additional effects originating from the surface magnetic layers being exchange coupled to only one neighboring magnetic layer while the interior magnetic layers are coupled to two neighboring layers. This makes a quantitative comparison difficult. In Fe/Cr(211) superlattices, this can give rise to two spin-flop transitions (bulk and sometimes also surface) when the applied field is parallel to the uniaxial anisotropy axis.[10]

The paper is structured as follows. Section II describes the experimental procedures. Section III contains experimental results. Section IV describes the data analysis of the magnetization, MR and BLS results, and includes details of the calculation of the spin-wave mode frequencies. Section V compares the results obtained with the different techniques. Section VI presents the results for (001) Fe/Cr/Fe trilayers. Finally Sec. VII contains discussions and conclusions.

II. EXPERIMENTAL PROCEDURES

The (211)-Fe/Cr samples were made by dc magnetron sputtering onto epitaxially polished single-crystal MgO(110)

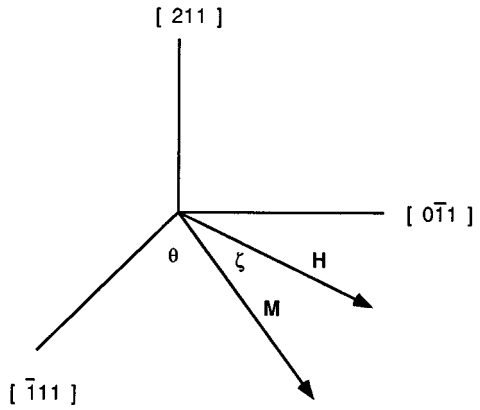

FIG. 1. Schematic diagram showing the orientation of M and H with respect to the Fe crystallographic orientation. The Fe[211] axis is normal to the layer, the hard $[\bar{1}11]$ and easy $[0\bar{1}1]$ axes lie in the layer plane. Although not shown in the figure, the magnetization is not constrained to lie in plane and forms an angle ϕ with the [211] axis.

substrates using the same growth procedure outlined for superlattices.[6] A 200-Å Cr(211) base layer was grown at 600 °C. The substrate was then cooled to ≈180 °C prior to the growth of a 20-Å Cr layer, and either a 20-Å Fe layer or an AF-coupled Fe(20 Å)/Cr(11 Å)/Fe(20 Å) trilayer which were then capped with a 20-Å Cr layer. The samples grow with the Fe $[\bar{2}11]$ along the surface normal and the in-plane $[\bar{1}11]$ and $[0\bar{1}1]$ directions parallel to MgO $[\bar{1}10]$ and [001], respectively. Magnetization studies have shown that the $[\bar{1}11]$ and $[0\bar{1}1]$ directions are the hard and easy axes, respectively. The coordinate system we use is shown in Fig. 1. We define θ and ζ as the angles that the magnetization (M) and the applied field (H), respectively, make with the hard axis in the plane of the film. ϕ is the angle the magnetization makes with the [211] axis (not shown in the figure). (100)-Fe/Cr samples were grown onto MgO(100) substrates simultaneously with the growth of the (211) samples; in the (100) samples the epitaxial orientation is Fe/Cr[001]‖MgO[011].

All measurements were done at room temperature. For each technique, both the easy- and hard-axis behavior of each sample was investigated. Magnetic hysteresis loops were measured by both longitudinal surface magneto-optical Kerr effect (SMOKE) and by SQUID magnetometry. The MR was measured using a standard, four-terminal dc technique. The spin-wave excitations were measured by BLS experiments using 250 mW of 5145-Å radiation from an Ar^+ laser. The scattered radiation was analyzed with a tandem Fabry-Perot interferometer[11] in 3+2 pass operation. The magnitude of the wave vector $q_\parallel$ in our experiments (determined from the scattering geometry) is 0.65×10^5 cm^{-1}. All techniques were used to study the same films; thereby eliminating any sample-to-sample variations.

III. EXPERIMENTAL RESULTS

Figure 2 shows hard-axis SMOKE results for a (211)-oriented 20-Å Fe film. Figures 3(a) and 3(b) show the Kerr effect and MR results, respectively, for the (211) Fe/Cr/Fe

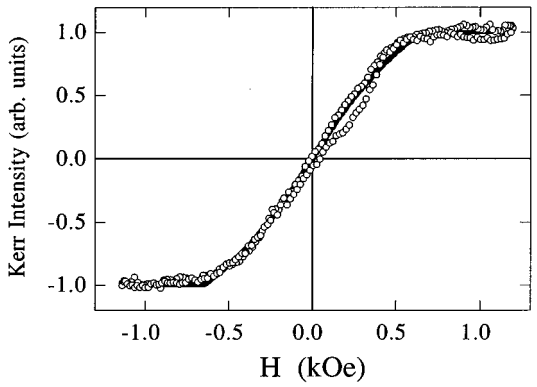

FIG. 2. SMOKE magnetization loop for H along the hard axis of the single (211)-Fe layer. Symbols are experimental points, the line is the fit described in the text. Parameters determined from the fit are given in Table I.

trilayer: the squares and circles denote experimental data for the hard and easy axes, while the solid lines are fits to be described below. The single Fe film exhibits the expected uniaxial anisotropy with the easy axis parallel to the Fe$\langle 0\bar{1}1\rangle$ axis. When H is applied along the easy axis, the Fe/Cr/Fe trilayer exhibits a spin-flop transition characteristic of a film in which there is a combination of AF coupling and uniaxial anisotropy. This can be seen as discrete jumps at $H\approx1.5$ kOe in both the magnetization and MR results. At low fields, the Fe layers are AF aligned along the easy axis. Higher fields induce a first-order phase transition in which

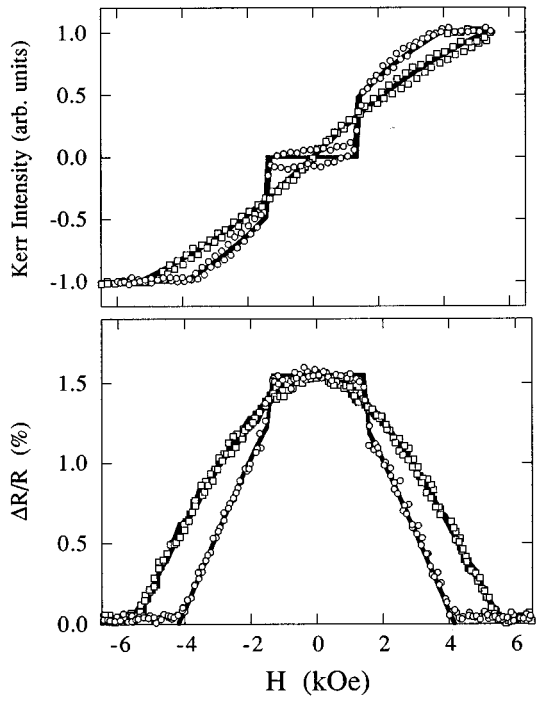

FIG. 3. Hard (squares) and easy (circles) axis magnetization (upper) and magnetoresistance (lower) loops for the (211)-Fe/Cr/Fe sample. Symbols are experimental points, the line is the fit described in the text. Parameters determined from the fits are given in Table I.

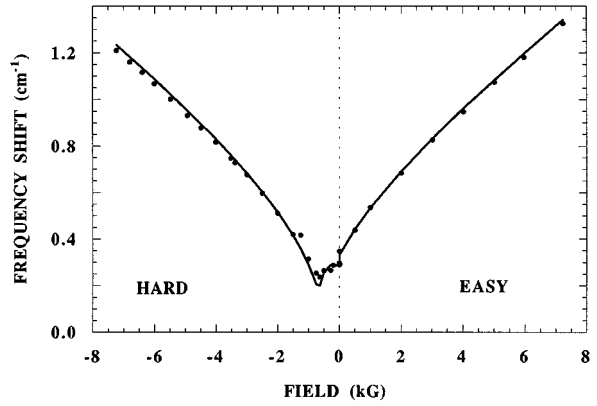

FIG. 4. Magnon frequency of a single (211)-Fe film for the field applied along the hard and easy directions. Symbols are experimental points, the line is the fit described in the text. For clarity the hard-axis results have been plotted along the negative field axis. Parameters determined from the fit are given in Table I.

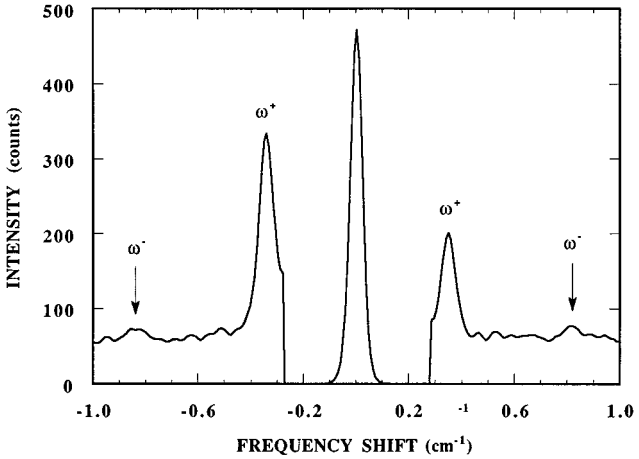

FIG. 5. Spectrum obtained from the (211)-Fe/Cr/Fe sample with $H=0.5$ kG along the hard axis. The arrows indicate the magnon peaks. The central peak is the unshifted radiation attenuated by $\approx 10^5$.

the spins switch from being antiparallel along the easy axis to the spin-flop phase in which the spins reorient almost 90° from the field direction but cant toward it. When H is along the hard axis, the Fe layers continuously rotate to saturation. In the quantitative analysis of the magnetization loops we will concentrate on SMOKE as opposed to SQUID results. Analysis of the SQUID results were complicated by the difficulty in uniquely separating the contributions from the substrate and/or sample holder from that of the Fe film. We found that the magnetic signal from the MgO substrate consisted of both a large diamagnetic response and a superparamagnetic signal which arises from impurities which saturates at ≈ 2000 Oe with a moment equivalent to $\approx 3-4$ Å of Fe.

BLS spectra from the single film show a single mode with asymmetric Stokes and anti-Stokes intensities, as expected. The magnon frequency, for H both along the easy and hard directions, is shown in Fig. 4; symbols are experimental points, lines are the fits to be described in the next section. The difference in the frequencies along the two field directions depends only on the anisotropy. Representative spectra of the trilayer film are shown in Fig. 5; they show two modes resulting from in-phase and out-of-phase oscillations of the two Fe layers. The intensity of the weak mode in Fig. 5 is only about 2% of that of the intense mode. In principle, since the weak mode is antisymmetric, the contribution to the scattering cross section of the two layers should exactly cancel. However, we believe that the small attenuation as light traverses the outer layers or small differences in the anisotropies of the two layers explains why the mode is observable.

The frequencies of the symmetric and antisymmetric modes plotted vs H are shown in Fig. 6. The difference at ''zero'' field between the magnon frequency of the upper mode for H along the hard and easy axes is real; it is due to the finite wave-vector correction, as discussed in the Appendix. The discontinuity in the frequencies at ≈ 1.5 kG with H along the easy axis reflects the spin-flop transition. The frequency minimum at ≈ 5 kG reflects the saturation field H_s.

IV. DATA ANALYSIS

We have fitted the field dependence of the magnetization, MR and BLS results to extract magnetic parameters. The values for the magnetization and MR depend on the equilibrium magnetic configuration which can be calculated by minimizing the total energy of the system. The magnon frequencies are obtained by calculating the perturbations of the layers from their equilibrium state. As a result of the large demagnetizing fields, the equilibrium condition corresponds to the Fe moments in the plane of the film ($\phi=90°$). However, since magnons involve the precession of the moments out of the plane, to properly treat the frequencies the three-dimensional total energy must be considered. Therefore, we first derive the most general energy expressions appropriate to BLS, and then simplify them when fitting the magnetization and MR data.

The energy (per unit volume) for a single (211)-Fe film,

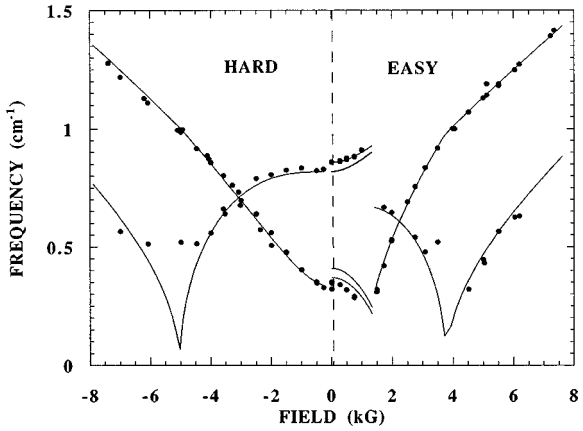

FIG. 6. Magnon frequencies of the (211)-Fe/Cr/Fe sample for the field applied along the hard and easy directions. Symbols are experimental points, the line is the fit described in the text. For clarity the hard-axis results have been plotted along negative field axis. Parameters determined from the fit are given in Table I.

which includes crystalline and uniaxial anisotropies, shape anisotropy and Zeeman terms, is given by

$$E_1 = K_1\left\{\frac{1}{4}\cos^4\phi + \frac{\sqrt{2}}{3}\cos^3\phi\cos\theta\sin\phi + \frac{1}{3}\sin^4\phi\cos^4\theta + \frac{1}{2}\cos^2\phi\sin^2\phi\sin^2\theta - \sqrt{2}\cos\phi\sin^3\phi\cos\theta + \frac{1}{4}\sin^4\phi\sin^4\theta\right\} + K_u\cos^2\theta + 2\pi M_s^2\cos^2\phi - HM_s\cos(\theta-\zeta)\sin\phi, \quad (1)$$

where K_1 is the cubic anisotropy constant, K_u is a uniaxial anisotropy constant characteristic of Fe(211) films, and M_s is the saturation moment of the layer. The angles are defined in Fig. 1. The unusual cubic-anisotropy term in Eq. (1) results from a rotation from the cubic axes in our reference frame.

The energy (per unit area) of the bilayer system is given by

$$E = d_1E_1 + d_2E_2 - J_1\mathbf{m}_1\cdot\mathbf{m}_2 - J_2(\mathbf{m}_1\cdot\mathbf{m}_2)^2, \quad (2)$$

where E_i and d_i are the energy densities and thicknesses, respectively, of layers $i=1,2$. The product $\mathbf{m}_1\cdot\mathbf{m}_2$ is given by

$$\mathbf{m}_1\cdot\mathbf{m}_2 = \sin\phi_1\sin\phi_2\cos(\theta_1-\theta_2) + \cos\phi_1\cos\phi_2. \quad (3)$$

A. Magnetization and magnetoresistance

The condition for equilibrium requires that the derivative of E with respect to all the angles must be zero. Because of the magnitude of the demagnetizing field in Eq. (1), it turns out that to a very good approximation, the equilibrium condition is $\phi=90°$. This condition greatly simplifies the energy expression which can be used to evaluate the magnetization and the MR, viz.,

$$E = \sum_{i=1}^{2} K_1d_i\left\{\frac{1}{3}\cos^4\theta_i + \frac{1}{4}\sin^4\theta_i\right\} + K_ud_i\cos^2\theta_i - HM_sd_i\cos(\theta_i-\zeta) - J_1\cos(\theta_1-\theta_2) - J_2\cos^2(\theta_1-\theta_2). \quad (4)$$

In general, we numerically minimize this equation to determine θ_1 and θ_2, and adjust the parameters to fit the experimental SMOKE and MR results. The magnetization and MR are proportional to $M_s(d_1\cos\theta_1 + d_2\cos\theta_2)$ and $1-\cos(\theta_1-\theta_2)$, respectively. However, for our particular sample with two equivalent Fe layers ($d_1=d_2=d$), the derivatives can be manipulated further to yield analytical expressions which are more convenient in understanding the reliability of the constants extracted. For H applied along the hard axis, the condition $\theta_1=-\theta_2$ holds for all fields. Substituting the value $|\theta_1|=|\theta_2|=\theta$ into the equilibrium condition $dE/d\theta=0$, we get the following expressions relating θ to H. For H less than $H_s=(-2J_1-4J_2+2dK_u+4dK_1/3)/M_sd$,

$$HM_sd = (-2J_1+4J_2+2dK_u-dK_1)\cos\theta + \left(-8J_2+\frac{7}{3}dK_1\right)\cos^3\theta. \quad (5)$$

Since the magnetization of the magnetic trilayer is given by $2M_sd\cos\theta$, and the MR is proportional to $1-\cos2\theta$, the anisotropies and interlayer coupling constants can be readily least-squares fitted to the experimental data. Trivial modifications to the above expressions ($J_1=J_2=0$) allow them to be used to describe the hard-axis magnetization of the single film (Fig. 2).

Similar arguments can be made for H applied along the easy axis. When $H<H_{SF}$, $\theta_1=90°$ and $\theta_2=-90°$; for $H>H_s=(-2J_1-4J_2-2dK_u+dK_1)/M_sd$ we have $\theta_1=\theta_2=90°$, and for $H_{SF}<H<H_s$ (and provided that J_2 is not too large, a condition satisfied by our sample) we have $\theta_1=180-\theta_2$ which leads to

$$HM_sd = \left(-2J_1+4J_2-2dK_u-\frac{4}{3}dK_1\right)\sin\theta + \left(-8J_2+\frac{7}{3}dK_1\right)\sin^3\theta. \quad (6)$$

It is clear from Eqs. (5) and (6) that if one of the parameters is smaller than all others (K_1 in our case) it is less likely to be extracted reliably from magnetization data since the parameters always appear in combination with J_2. Note also that Eqs. (5) and (6) contain only three distinct combinations of parameters; it is therefore unreasonable to attempt to extract more than three parameters from fits to these expressions.

B. Brillouin light scattering

There have been many derivations of magnon frequencies in coupled layer systems.[12–14] However, in order to guarantee that the approximations made in describing the magnetization are identical to those used to describe the BLS, we derived the BLS frequencies starting from the same energy expression we used to derive the magnetization and MR. This approach guarantees that any discrepancies between the BLS and magnetization results cannot be attributed to inconsistent forms of the energy expression.

The formalism which we use to calculate the Brillouin frequencies basically follows that described Cochran *et al.*[12] By using this approach we implicitly assume that (i) there is no domain formation, and (ii) effects of intrafilm exchange are negligible. These approximations are expected to be valid because the Fe layers are so much thinner than the wavelengths of the excitations probed.[15] The magnon modes probed with BLS typically have a wave-vector component parallel to the surface of order of $2\pi/\lambda$, where λ is the wavelength of light. An exact calculation of such modes can be performed,[16] but requires extensive use of numerical techniques in all but the simplest cases. Since solutions obtained by numerical methods make fitting procedures unwieldy, such solutions are not particularly useful when one desires to extract the physical constants from the experimental data. Approximate analytical expressions for the magnon frequen-

TABLE I. Parameters extracted for (211) single film and coupled trilayers. Asterisks indicate parameters which are fixed during fitting.

	K_1 ($\times 10^5$ ergs/cm^3)	K_u ($\times 10^5$ ergs/cm^3)	$4\pi M_s$ (kG)	J_1 (ergs/cm^2)	J_2 (ergs/cm^2)
		Single (211)-Fe layer			
SMOKE	1.1 ± 0.5	4.6 ± 0.2			
BLS	1.1*	4.6 ± 0.2	16.5 ± 0.5		
		(211)-Fe/Cr/Fe layers			
SMOKE	1.1*	5.6 ± 0.3		-0.64 ± 0.02	-0.045 ± 0.010
MR	1.1*	5.6 ± 0.3		-0.69 ± 0.02	-0.038 ± 0.013
BLS ω^+	1.1*	5.0 ± 0.3	18.0 ± 0.1		
BLS ω^-	1.1*	5.0*	18*	-0.61 ± 0.02	-0.038 ± 0.013

cies which we use to least-squares fit to the experimental results are outlined in the Appendix.

In all our fits to the BLS data we use the bulk Fe value of $\gamma=2.93$ GHz/kG. We emphasize that in fitting the data to Eqs. (A7) it is necessary to evaluate Eqs. (A8) at the equilibrium angles. In our case this can be done analytically through Eqs. (5) and (6).

C. Errors

The equations obtained above allow least-squares fits to be performed on each of the data sets. Determining the confidence level of parameters thus extracted, especially when strong correlations exist between parameters, is often not addressed in the literature. It therefore deserves some attention. First the data were fitted with all parameters as variables, and the mean-square deviation calculated. Second, each parameter in turn was varied by a small amount and the data refit with that parameter held fixed. The change which led to an increase of $\approx 50\%$ in the mean-square deviation was chosen as the confidence level of the parameter in question. We chose the somewhat arbitrary 50% increase because this typically leads to a visibly discernible deterioration of the fit.

V. COMPARISON OF RESULTS

All the curves in the figures presented in Sec. III correspond to least-squares fits to the data. Excellent fits are obtained for all the data sets. The question we wish to address here is that of self-consistency of the various determinations, both between the single film and the coupled trilayers and between the different experimental techniques.

Table I contains the parameters extracted from the single (211)-Fe and coupled (211)-trilayer films. To evaluate K and J in Table I we have used $M=1.6$ kG and $d=20$ Å . We begin the comparison by stressing that we expect the relevant properties of the single film to be close to those of the individual films in the coupled layers. From the magnetization loops for the single film, we can determine the cubic anisotropy K_1 [Eq. (5) with $J_1=J_2=0$]. It turns out however that the effects of cubic anisotropy are small and it is not possible to extract a reliable value for K_1 from any of our other measurements. Therefore, we have simply fixed the value of K_1 in fitting all other data sets.

The reliability of the parameters extracted depends to some degree on how the data are fitted. Fitting separately the single-film BLS data along the hard and easy axes yields two values of K_u, both with large uncertainties. However, fitting both data sets simultaneously produces a single value of K_u with its uncertainty considerably reduced. Therefore, we fit the hard- and easy-axis data simultaneously for all data sets. We separately fit the ω^+ and ω^- modes in order to isolate the contribution of interlayer coupling from that of the anisotropy; ω^+ senses only the anisotropy [Eq. (A7a)] while ω^- depends on both the interlayer coupling and anisotropy [Eq. (A7b)].

The values for J_1 and J_2 determined from SMOKE, MR, and BLS are in reasonable agreement; the largest discrepancy is between the BLS and MR values of J_1 which are slightly outside the estimated error bars. The values of J_2 are self-consistent and considerably smaller than J_1. Although J_2 is small, it proved impossible to quantitatively fit any of the data without including it in the energy expression. Our values for K_u determined using the different techniques agree with each other for a given sample, but are slightly outside estimated uncertainties when comparing the trilayer to the single film. Both the anisotropy and J_1 are consistent with previous superlattice results.[6] Our values of $4\pi M_s$ are in the range reported for 20-Å Fe films. There is, however, a small difference between the $4\pi M_s$ values for the single and trilayers which is puzzling. This difference could be real and due to subtle growth effects which give rise to different perpendicular surface anisotropies, or could be an artifact of the approximations made in deriving the magnon frequencies.

VI. Fe/Cr/Fe (100) TRILAYERS

Having established that accurate numerical values can be extracted using the techniques mentioned above, we also measured a single Fe film and a coupled trilayer which were deposited onto MgO (100) substrates simultaneously with the samples discussed above. The energy equation which includes the crystalline anisotropy, Zeeman, and interlayer coupling terms is

$$E=\sum_{i=1}^{2}\frac{1}{4}K_1 d_i \sin^2(2\theta_i)-HM_s d_i\cos(\theta_i-\zeta)$$
$$-J_1\cos(\theta_1-\theta_2)-J_2\cos^2(\theta_1-\theta_2). \quad (7)$$

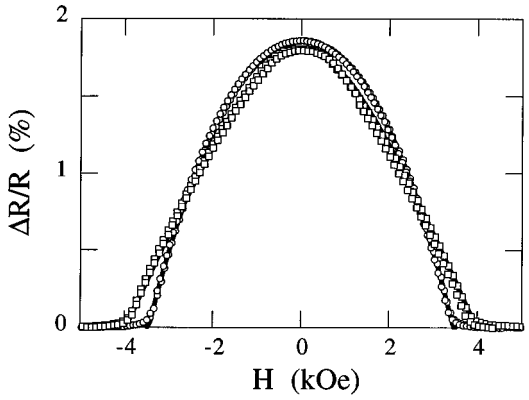

FIG. 7. Hard-(squares) and easy-(circles) axis magnetoresistance for the (100)-Fe/Cr/Fe sample. Symbols are experimental points, the line is the fit described in the text. Parameters determined from the fit are given in Table II.

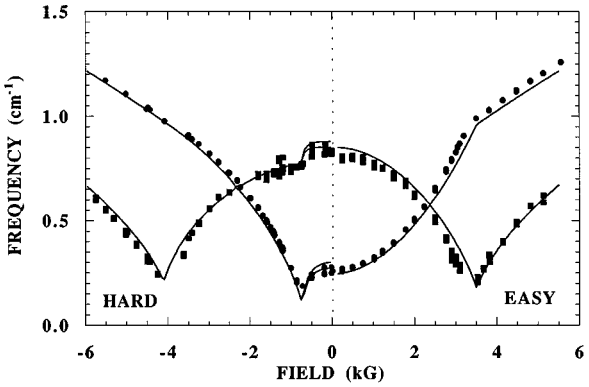

FIG. 8. Magnon frequencies of the (100)-Fe/Cr/Fe sample for the field applied along the hard and easy directions. Symbols are experimental points, the line is the fit described in the text. For clarity the hard-axis results have been plotted along negative field axis. Parameters determined from the fit are given in Table II.

Even though the energy expression for this orientation is simpler (a fourfold anisotropy term and $K_U=0$) the magnetic phase diagram is more complex since there are now four easy directions for the magnetization of each layer. Nonetheless, following basically the same procedure as outlined above for the (211) samples, we have extracted the magnetic parameters for the (100) films from the BLS and MR data.

The measurements were performed with the field along the easy-axis [001] and hard-axis [011] in-plane directions. The MR results are shown in Fig. 7, and the parameters of the least-squares fit are given in Table II. The difference in the saturation fields in Fig. 7 reflects the contribution of the crystalline anisotropy. Figure 8 shows the magnon frequencies and fits for the coupled (100) trilayer. The MR results are compared with the BLS results in Table II. The two techniques give the same values for both the anisotropy and interlayer coupling. The largest discrepancy is in the determination of J_2, but the values are still just within the estimated uncertainties.

VII. DISCUSSION AND CONCLUSIONS

In comparing the results for (211)- and (100)-coupling strengths we see that the values for J_1 are very similar for the two orientations. This agrees with previous superlattice studies.[6] The results for J_1 are also in agreement with recent measurements on Fe/Cr/Fe(100) trilayers by Heinrich *et al.*[15] and Grünberg *et al.*[17] and with the results of Elmers *et al.*[9] and Parkin *et al.*[18] on Cr(110) spacer layers. Most studies of the bilinear interlayer coupling in Fe/Cr systems report a maximum value of $J_1 \approx -1$ erg/cm^2 for Cr thickness of ≈ 8 Å , which appears to be independent of the crystallographic orientation. There are, however, some reports of lower J_1 values in Fe/Cr/Fe(100) trilayers.[8,14,19,20]

In contrast to the bilinear coupling for which J_1 is similar for the two orientations, it is surprising that the biquadratic coupling is considerably higher in the (211) sample than in the (100) sample. Although we find the biquadratic coupling to be quite small for the (100) sample investigated here, in similarly grown (100) superlattices with thicker Cr layers, the biquadratic coupling can dominate the bilinear coupling.[21]

In comparing to the literature values for J_2, there is considerable spread in the reported values for the Fe/Cr(100) system,[15,17,19,20,22] and the values of J_2 are sensitive to details of the growth conditions.[23,24] Elmers *et al.*[9] observe large values of J_2 in Fe/Cr/Fe(110) trilayers for thin Cr spacers. These results suggest that an extrinsic mechanism which depends sensitively on the interfacial structure is controlling the magnitude of J_2. In Slonczewski's[4] fluctuation model, the relevant structural parameter is the lateral length of atomically smooth Cr layer terraces. This could explain the larger J_2 values observed in the samples in which the short-

TABLE II. Parameters extracted for (100) single-film and coupled trilayers. Asterisks indicate parameters which are fixed during fitting.

	K_1 ($\times 10^5$ ergs/cm^3)	$4\pi M_s$ (kG)	J_1 (ergs/cm^2)	J_2 (ergs/cm^2)
		Single Fe layer		
BLS	2.2 ± 0.3	20.6 ± 0.3		
		Double Fe layer		
MR	2.4 ± 0.3		-0.57 ± 0.02	-0.016 ± 0.013
BLS ω^+	2.2 ± 0.2	19.8 ± 0.1		
BLS ω^-	2.2*	19.8*	-0.57 ± 0.02	-0.003 ± 0.003

period oscillations are also observed.[15,17] The model may not be applicable to the (211)-oriented sample in which short period oscillations, although theoretically predicted,[7] have not been observed. Careful measurement of the thickness and temperature dependence of the biquadratic coupling in (211) coupled samples are needed to further understand its origin.

In conclusion, we have used BLS in conjunction with magnetization and magnetoresistance techniques to study (211)- and (100)-Fe/Cr/Fe trilayers. We find that the coupling strengths extracted using each technique are self-consistent. This not only provides reliable values for the coupling strengths but also highlights the complementarity of these techniques in uniquely determining the magnetic parameters. In particular, combining magnetization measurements (which are proportional to the net magnetization in the field direction) and the MR (which is proportional to the cosine of the angle between the magnetization of the layers) allows one to uniquely extract the magnetic configuration as a function of applied field. This proves particularly useful in analyzing films where the two magnetic layers have different thicknesses and/or anisotropies.

ACKNOWLEDGMENTS

We wish to thank Dr. S. Bader for helpful discussions and a critical reading of the manuscript. This work was supported by U.S. Department of Energy, Basic Energy Sciences-Materials Sciences under Contract No. W-31-109-ENG-38.

APPENDIX

In this appendix we outline the approach to calculate analytical expressions for the spin-wave frequencies for single layers and coupled trilayers.

1. Single layer

It is known[25] that the FMR frequency, which corresponds to the infinite wavelength magnon, is obtained by solving

$$\begin{vmatrix} E_{\theta\theta} & E_{\theta\phi}-i\omega M_s/\gamma\sin\phi \\ E_{\theta\phi}+i\omega M_s/\gamma\sin\phi & E_{\phi\phi} \end{vmatrix}=0, \quad \text{(A1)}$$

where $E_{\theta\theta}$, $E_{\theta\phi}$, and $E_{\phi\phi}$ are the second derivatives of the energy (per unit volume) given in Eq. (1) with respect to the angles indicated in the subscript, and γ is the gyromagnetic ratio. Since our Fe layers are only 20-Å thick, the correction which must be included to account for the finite wavelength of the magnons probed by Brillouin scattering can be treated as a perturbation. Following the approach of Cochran *et al.* it can be shown that for magnon wave vectors (q) perpendicular to the applied field, and to lowest-order terms in qd, the following terms

$$\begin{vmatrix} 2\pi M_s^2 qd\cos^2(\theta-\zeta) & 0 \\ 0 & -2\pi M_s^2 qd \end{vmatrix} \quad \text{(A2)}$$

must be added to Eq. (A1).

The general solution for the field along the hard axis, which includes the region below saturation, where M and H are not parallel, is

$$\begin{aligned}(\omega/\gamma)^2=&\left[H\cos\theta-\frac{2K_U}{M_S}(1-2\sin^2\theta)\right.\\&\left.+\frac{K_1}{3M_S}[29\sin^2\theta-28\sin^4\theta-4]\right]\\&\times\left[H\cos\theta+4\pi M_S+\frac{K_1}{3M_S}[11\sin^2\theta-7\sin^4\theta-4]\right]\\&-2\left(\frac{K_1}{M_S}\right)^2[9\sin^6\theta-12\sin^4\theta+4\sin^2\theta]\\&+(2\pi M_S)^2 2qd\cos^2\theta. \quad \text{(A3)}\end{aligned}$$

In order to obtain the field dependence of ω one must also use Eqs. (5) and (6) which relate θ to H.

For the field along the easy axis, $\theta=\phi=90°$ for all fields and the expression for frequency is given by

$$\begin{aligned}(\omega/\gamma)^2=&\left(H+\frac{2K_U}{M_S}-\frac{K_1}{M_S}\right)(H+4\pi M_S)\\&-2\left(\frac{K_1}{M_S}\right)^2+(2\pi M_S)^2 2qd. \quad \text{(A4)}\end{aligned}$$

2. Double layer

The general expression for the frequencies of the FMR modes of a double layer can be obtained by solving the following 4×4 determinant derived from the equations of motion (assuming $\phi_1=\phi_2=90°$ and $d_1=d_2=d$):

$$\begin{vmatrix} E_{\theta_1\theta_1} & E_{\theta_1\phi_1}-i\omega M_s/\gamma & E_{\theta_1\theta_2} & E_{\theta_1\phi_2} \\ E_{\phi_1\theta_1}+i\omega M_s/\gamma & E_{\phi_1\phi_1} & E_{\phi_1\theta_2} & E_{\phi_1\phi_2} \\ E_{\theta_2\theta_1} & E_{\theta_2\phi_1} & E_{\theta_2\theta_2} & E_{\theta_2\phi_2}-i\omega M_s/\gamma \\ E_{\phi_2\theta_1} & E_{\phi_2\phi_1} & E_{\phi_2\theta_2}+i\omega M_s/\gamma & E_{\phi_2\phi_2} \end{vmatrix}=0, \quad \text{(A5)}$$

where again $E_{\theta_k\theta_k}$, $E_{\phi_k\phi_k}$, and $E_{\theta_k\phi_k}$ (with $k=1,2$ corresponding to layer 1 or 2) are the second-order derivatives of energy (per unit volume) with respect to the angles indicated in the subscript. The finite-wave-vector effects can be included for this case

by following an approach similar to that of the single layer. Keeping only the lowest-order terms in qd, the following matrix must be added to Eq. (A5):

$$2\pi M_s^2 qd \begin{vmatrix} \cos^2(\theta_1-\zeta) & 0 & \cos(\theta_1-\zeta)\cos(\theta_2-\zeta) & i\cos(\theta_1-\zeta) \\ 0 & -1 & i\cos(\theta_2-\zeta) & -1 \\ \cos(\theta_1-\zeta)\cos(\theta_2-\zeta) & -i\cos(\theta_2-\zeta) & \cos^2(\theta_2-\zeta) & 0 \\ -i\cos(\theta_1-\zeta) & -1 & 0 & -1 \end{vmatrix}. \tag{A6}$$

In our symmetric bilayer there are some additional simplifications which allow us to extract analytical expressions for the frequencies. For all fields, when $H\|[-111]$ (hard axis) we have $\theta_1=-\theta_2$; when $H\|[0-11]$ (easy axis) and for fields above H_{SF} we have $\theta_1=180-\theta_2$; both of these conditions lead to the simplification $E_{\theta_1\theta_1}=E_{\theta_2\theta_2}=E_{\theta\theta}$, $E_{\phi_1\phi_1}=E_{\phi_2\phi_2}=E_{\phi\phi}$, $E_{\theta_1\phi_1}=E_{\theta_2\phi_2}$.

The above conditions and the inversion symmetry of our sample, that requires that the solutions of Eq. (A5) be either symmetric or antisymmetric, enable us to reduce the determinant from a 4×4 to a 2×2, and consequently to obtain analytical solutions. [Note that Eq. (A5), plus Eq. (A6) does not have exact symmetric and antisymmetric solutions. However, because Eq. (A6) is small, the corrections are quadratic. Also the inversion symmetry condition does not hold for $H<H_{SF}$ when H is applied along the easy axis.] The expansion of the determinant (keeping only the first-order terms in qd) leads to a quadratic equation in ω^2 whose solutions are

$$(\omega_+/\gamma)^2=[(E_{\theta\theta}+E_{\theta_1\theta_2})E_{\phi\phi}-E_{\theta\phi}^2]+\cos^2(\theta-\zeta)\times(4\pi M_s)^2qd, \tag{A7a}$$

$$(\omega_-/\gamma)^2=[E_{\theta\theta}-E_{\theta_1\theta_2}]E_{\phi\phi}-E_{\theta\phi}^2, \tag{A7b}$$

where $\theta=\theta_1=-\theta_2$ for $H\|[\bar{1}11]$ and $\theta=\theta_1=180-\theta_2$ for $H\|[0\bar{1}1]$ and ζ is the angle between H and $[111]$. [Equation (A7) is not valid below H_{SF} when H is applied along the easy axis.] The second derivatives of energy can be written as

$$E_{\theta\theta}=H\cos(\theta-\zeta)-\frac{2K_U}{M_S}(2\cos^2\theta-1)+\frac{K_1}{3M_S}(-28\cos^4\theta+27\cos^2\theta-3)-E_{\theta_1\theta_2}, \tag{A8a}$$

$$E_{\theta_1\theta_2}=\{-J_1\cos2\theta-2J_2[(\cos^2\theta-\sin^2\theta)^2-4\cos^2\theta\sin^2\theta]\}/d \tag{A8b}$$

$$E_{\phi\phi}=H\cos(\theta-\zeta)+4\pi M_S+\frac{K_1}{3M_S}(3\cos^2\theta-7\cos^4\theta), \tag{A8c}$$

and

$$E_{\theta\phi}^2=2\left(\frac{K_1}{M_S}\right)^2\sin^2\theta(3\cos^2\theta-1)^2. \tag{A8d}$$

The frequencies of the two modes can be calculated from Eqs. (A7a) and (A7b) by setting $\zeta=0$ and 90° for the hard and easy axes, respectively, and by using Eqs. (5) and (6) to calculate θ as a function of H.

[1] See articles in *Ultrathin Magnetic Structures I and II*, edited by J. A. C. Bland and B. Heinrich (Springer, New York, 1994).

[2] M. Rührig, R. Schäfer, A. Hubert, R. Mosler, J. A. Wolf, S. Demokritov, and P. Grünberg, Phys. Status Solidi A **125**, 635 (1991).

[3] C. J. Gutierrez, J. J. Krebs, M. E. Filipkowski, and G. A. Prinz, J. Magn. Magn. Mater. **116**, L305 (1992).

[4] J. C. Slonczewski, J. Magn. Magn. Mater. **150**, 13 (1995), and references therein.

[5] S. Demokritov, E. Tsymbal, P. Grünberg, W. Zinn, and I. K. Schuller, Phys. Rev. B **49**, 720 (1994).

[6] E. E. Fullerton, M. J. Conover, J. E. Mattson, C. H. Sowers, and S. D. Bader, Phys. Rev. B **48**, 15 755 (1993).

[7] D. D. Koelling, Phys. Rev. B **50**, 273 (1994).

[8] J. J. Krebs, P. Lubitz, A. Chaiken, and G. A. Prinz, Phys. Rev. Lett. **63**, 1645 (1989).

[9] H. J. Elmers, G. Liu, H. Fritzsche, and U. Gradmann, Phys. Rev. B **52**, R696 (1995).

[10] R. W. Wang, D. L. Mills, E. E. Fullerton, J. E. Mattson, and S. D. Bader, Phys. Rev. Lett. **72**, 920 (1994).

[11] J. R. Sandercock, in *Light Scattering in Solids III*, edited by M. Cardona and G. Güntherodt (Springer, Berlin, 1982), p. 173.

[12] J. F. Cochran, J. Rudd, W. B. Muir, B. Heinrich, and Z. Celinski, Phys. Rev. B **42**, 508 (1990).

[13] M. Macció, M. G. Pini, P. Politi, and A. Rettori, Phys. Rev. B **49**, 3283 (1994).

[14] P. Kabos, C. E. Patton, M. O. Dima, D. B. Church, R. L. Stamps, and R. E. Camley, J. Appl. Phys. **75**, 3553 (1994).

[15] B. Heinrich and J. F. Cochran, Adv. Phys. **42**, 423 (1993).

[16] B. Hillebrands, Phys. Rev. B **41**, 530 (1990).

[17] P. A. Grünberg, A. Fuss, Q. Leng, R. Schreiber, and J. A. Wolf, in *Magnetism and Structure in Systems of Reduced Dimension*, edited by R. F. C. Farrow *et al.* (Plenum, New York, 1993), p. 87.

[18] S. S. P. Parkin, N. More, and K. P. Roche, Phys. Rev. Lett. **64**, 2304 (1990).

[19] R. J. Hicken, C. Daboo, M. Gester, A. J. R. Ives, S. J. Gray, and J. A. C. Bland, J. Appl. Phys. **78**, 6670 (1995).
[20] C. D. Potter, R. Schad, P. Beliën, G. Verbanck, V. V. Moshchalkov, Y. Bruynseraede, M. Schäfer, R. Schäfer, and P. Grünberg, Phys. Rev. B **49**, 16 055 (1994).
[21] E. E. Fullerton, K. T. Riggs, C. H. Sowers, S. D. Bader, and A. Berger, Phys. Rev. Lett. **75**, 330 (1995).
[22] U. Köbler, K. Wagner, R. Wiechers, A. Fuß, and W. Zinn, J. Magn. Magn. Mater. **103**, 236 (1992).
[23] A. Schreyer, J. F. Ankner, Th. Zeidler, H. Zabel, M. Schäfer, J. A. Wolf, P. Grünberg, and C. F. Majkrzak, Phys. Rev. B **52**, 16 066 (1995).
[24] B. Heinrich (private communication).
[25] J. Smit and H. G. Beljers, Philips Res. Rep. **10**, 113 (1955).